14th International Symposium on Turbulence and Shear Flow Phenomena (TSFP14)
Heidelberg, Germany, July 28–31, 2026

A NON-DIMENSIONAL PARAMETER CHARACTERIZING THE RELAMINARIZATION OF TURBULENT BOUNDARY LAYERS AT SUPERSONIC EXPANSION CORNERS

Soju Maejima
Department of Aerospace Engineering, Graduate School of Engineering
Tohoku University
6-6-01, Aramaki Aza Aoba, Aoba-ku, Sendai, Miyagi, Japan
soju.maejima@dc.tohoku.ac.jp

Soshi Kawai
Department of Aerospace Engineering, Graduate School of Engineering
Tohoku University
6-6-01, Aramaki Aza Aoba, Aoba-ku, Sendai, Miyagi, Japan
kawai@tohoku.ac.jp

ABSTRACT

We investigate the relaminarization of supersonic turbulent boundary layers at expansion corners by direct numerical simulations for a range of Reynolds number, Mach number, and deflection angle conditions. Contrary to the established criterion based on Narasimha's parameter (Narasimha & Viswanath (1975)), relaminarization was observed even for the computed flow conditions in the reportedly "non-relaminarizing" regime. Through the budget analysis of the turbulent kinetic energy (TKE), we develop a model for the TKE decrease ratio across the expansion fan. The model shows good agreement with the measured TKE decrease for the wide range of flow conditions considered in this study.

INTRODUCTION

Under certain Reynolds and Mach number conditions, supersonic turbulent boundary layers at expansion corners are known to experience relaminarization due to the favorable pressure gradient from the expansion fan. The relaminarization can affect the aerodynamic performance of supersonic aircraft and rocket fairings, including but not limited to lower skin friction coefficients and significant differences in the further downstream flow phenomena. It is therefore crucial to accurately predict the occurrence and the extent to which relaminarization occurs for a given flow condition and geometry to realize an efficient and safe design in the aerospace industry.

An empirical condition for the relaminarization phenomenon was given by Narasimha & Viswanath (1975), now called Narasimha's parameter. By taking the ratio of the pressure change at the expansion corner Δp and the wall shear stress without the influence of the corner τ_{w0}, it was reported that relaminarization occurs when $\Delta p/\tau_{w0} > 75$ and does not when $\Delta p/\tau_{w0} < 60$. However, more recent studies report the occurrence of relaminarization below the lower bound of $\Delta p/\tau_{w0} < 60$ (Goldfeld *et al.* (2002); Nguyen *et al.* (2013); Pandey *et al.* (2024)), suggesting the necessity for further investigation into the condition for relaminarization.

Notably, Teramoto *et al.* (2017) and Sun *et al.* (2017) performed the budget analyses of the turbulent kinetic energy (TKE) and revealed that a negative contribution from the production term of the TKE budget at the expansion corner is the chief cause for the rapid attenuation of the turbulent fluctuations. In contrast, the incompressible flow under a favorable pressure gradient does not present such large negative contribution of the production term (Volino (2020)). This particular phenomenon that is unique to supersonic expansion leads us to believe that Narasimha's parameter, which is originally an extension of an existing parameter for relaminarization for incompressible flow, is not applicable to the present relaminarization mechanism at supersonic expansion corners.

In this study, we conduct the direct numerical simulations (DNS) of relaminarizing turbulent boundary layers at expansion corners to clarify the extent to which relaminarization occurs for varying flow conditions. In particular, we focus our analysis on the reduction of the turbulent kinetic energy as the indicator of relaminarization. Furthermore, from the budget equation of the TKE, we derive and propose a non-dimensional parameter that quantifies the decrease in the turbulent fluctuations solely from the flow conditions.

COMPUTATIONAL SETUP

The present DNS study directly solves the compressible Navier–Stokes equations with respect to the conservative variables (density, momentum, and total energy) using a well-validated in-house solver. The sixth-order compact differencing scheme (Lele (1992)) is employed for spatial discretization with the eighth-order compact filter (Lele (1992); Gaitonde & Visbal (2000)). The third-order TVD Runge–Kutta method (Gottlieb & Shu (1998)) is employed for time integration.

The Reynolds number based on the momentum thickness at the inlet is set to $Re_\theta = 1000$, 3000, 5000. Three freestream Mach numbers are chosen for each Reynolds number according to Narasimha's parameter to compute the reportedly "relaminarizing", "non-relaminarizing", and "in-between" cases

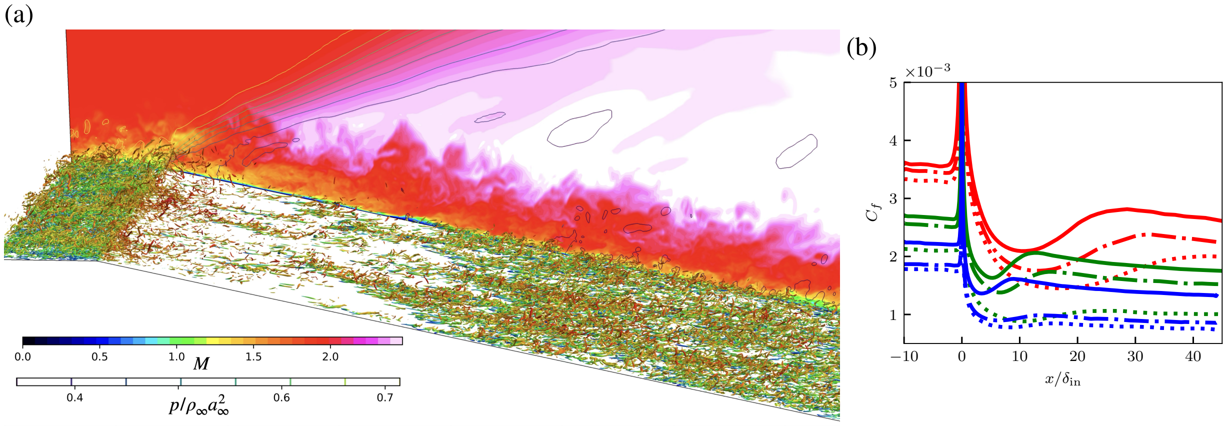

Figure 1. (a) Iso-surface of Q-criterion at $Q/(u_\infty/\delta_{\mathrm{in}})^2 = 15$, colored by local Mach number for $Re_\theta = 5000$, $M = 2$, $\alpha = 12°$ case. Background filled contour shows spanwise slice of local Mach number and contour lines show pressure. (b) Skin friction coefficients for nine cases with $\alpha = 12°$. Red, $Re_\theta = 1000$; green, $Re_\theta = 3000$; blue, $Re_\theta = 5000$. Solid lines, $\Delta p/\tau_{w0} > 75$ (low Mach); dash-dotted lines, $60 < \Delta p/\tau_{w0} < 75$ (medium Mach); dotted lines, $\Delta p/\tau_{w0} < 60$ (high Mach).

as in Table 1. The adiabatic non-slip wall condition is employed with the $\alpha = 12°$ expansion corner located at the streamwise location $x = 0$. We additionally perform the $Re_\theta = 1000$ computations with deflection angles of $\alpha = 3 \sim 11°$ in $1°$ increments for the same three Mach numbers to investigate the cases with weaker expansion and relaminarization. The inlet boundary condition at $x/\delta_{in} = -10$ is generated using a separate driver zone with the rescale-reintroduction method (Urbin & Knight (2001)), where δ_{in} is the inflow 99% boundary layer thickness. The computational domain is $-10 \leqq X/\delta_{in} \leqq 45$, $0 \leqq Y/\delta_{in} \leqq 100$, and $0 \leqq Z/\delta_{in} \leqq 6$. Here, the (x, y, z) axes denote the global cartesian axes and the (X, Y, Z) axes are rotated to align the wall after the corner. For the $Re_\theta = 1000$ and 3000 cases, the streamwise domain is extended to $-10 \leqq X/\delta_{in} \leqq 75$ to appropriately capture the boundary layers' return to equilibria after the expansion corner. The grid resolutions satisfy $\Delta X^+ \lesssim 10$, $\Delta Y^+_{\mathrm{min}} \lesssim 0.3$, and $\Delta Z^+ \lesssim 5$, where the + superscript denotes nondimensionalization by the wall unit. At the expansion corner, a finer streamwise grid resolution is used to satisfy $\Delta X/\delta_{in} = 10^{-3}$. The grid convergence is tested for the examined turbulence statistics, which did not show significant differences when a 1.5-times coarser computational grid was used.

Table 1. Freestream Mach numbers of computed cases

Re_θ	$\frac{\Delta p}{\tau_{w0}} > 75$ (Low Mach)	$60 < \frac{\Delta p}{\tau_{w0}} < 75$ (Medium Mach)	$\frac{\Delta p}{\tau_{w0}} < 60$ (High Mach)
1000	1.5	1.75	2
3000	1.75	2	2.75
5000	2	2.75	3

RESULTS AND DISCUSSION

Instantaneous flowfield and turbulence statistics

The iso-surface of the Q-criterion with the spanwise slice of the Mach number and pressure distributions for the $Re_\theta = 5000$, $M = 2$ (low Mach) case are shown in Figure 1(a). The pressure contours show that the expansion fan is formed originating from the expansion corner, yielding the pressure gradient and acceleration. The turbulent vortices in the incoming boundary layer are observed to decrease just after the expansion corner, which is indicative of relaminarization. Further downstream, the turbulent motions begin to regenerate and eventually reaches a turbulent state again. In the relaminarized region, the mach number distribution also shows that the near-wall fluctuations are attenuated forming a thin shear layer, demonstrated by the limited amount of disturbances in the low-speed (blue to green contours) near-wall region. The skin friction coefficient distributions for the nine computed cases with $\alpha = 12°$ are shown in Figure 1(b). At the expansion corner $x/\delta_{in} = 0$, the wall shear stress momentarily increases sharply due to the acceleration in the near-wall region, then decreases to a value lower than the initial turbulent values of $x/\delta_{in} < 0$. This decrease in the skin friction is another indication of relaminarization. The same trend of the skin friction development is observed for all nine cases, which suggests that the boundary layer experiences relaminarization to a certain extent even for the low Narasimha's parameter (high Mach number) cases as also suggested by existing studies (Goldfeld *et al.* (2002); Nguyen *et al.* (2013); Pandey *et al.* (2024)). The skin friction begins to increase after the local minimum indicating the retransition to a turbulent state, and eventually reaches a nearly flat profile.

The distributions of the mean wall-parallel velocity and turbulent kinetic energy (TKE) for the $Re_\theta = 5000$, $M = 2$ (low Mach) case are shown in Figure 2. Note that the velocity components (U, V, W) are those along the rotated coordinate system (X, Y, Z). The mean wall-parallel velocity shows the acceleration due to the expansion fan and the boundary layer profile noticeably changes from the incoming turbulent boundary layer, which suggests relaminarization. The TKE of the boundary layer shows a rapid and significant decrease at the expansion corner, reaching $20 \sim 30\%$ of its original value. Near the wall, the TKE begins to regenerate at $x/\delta_{\mathrm{in}} \approx 1$, while the outer layer away from the wall largely remains relaminarized. Figure 3 shows the distributions of the TKE for cases with $\alpha = 12°$. All nine cases show the rapid reduction of the TKE representing the occurrence of the relaminarization phenomenon, as was also observed from the skin coefficient distribution in Figure 1(b). Additionally, the high Mach cases

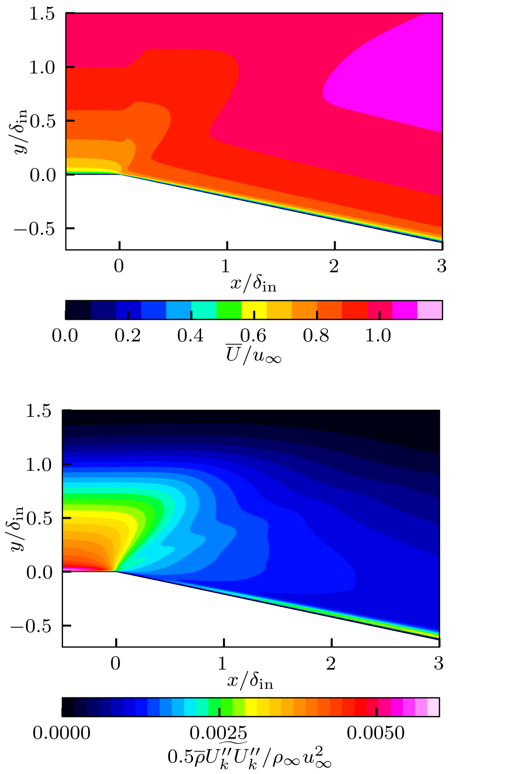

Figure 2. Distributions of mean wall-parallel velocity (top) and turbulent kinetic energy (bottom) for $Re_\theta = 5000$, $M = 2$, $\alpha = 12°$ case.

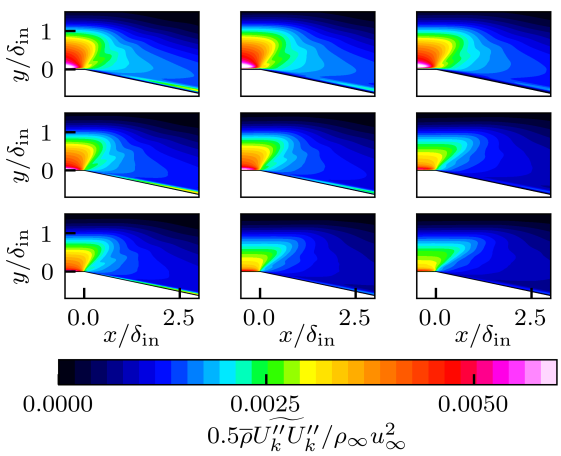

Figure 3. Distributions of turbulent kinetic energy for cases with $\alpha = 12°$. Top, $Re_\theta = 1000$; middle , $Re_\theta = 3000$; bottom, $Re_\theta = 5000$. Left, low Mach; center, medium Mach; right, high Mach.

(right column) seem to exhibit more significant TKE reductions compared to the low Mach number bases (left column).

To quantify the decrease in the TKE, we compare the ratios between the TKE values before and after the expansion along a given streamline. As demonstrated in Figure 4, for a given height y^{+0} at $x/\delta_{\rm in} = -2.5$, the pre-expansion TKE $\bar{\rho}\widetilde{K}\big|_{\rm pre}$ is taken at the streamwise location $x/\delta_{\rm in} = -2.5$, while the post-expansion TKE $\bar{\rho}\widetilde{K}\big|_{\rm post}$ is taken as the minimum TKE along the streamline (blue arrow) starting at $x/\delta_{\rm in} = -2.5$. Here the superscript $(\cdot)^{+0}$ signifies nondimensionalization using τ_{w0}, and $\widetilde{K} := \frac{1}{2}\widetilde{U_k''U_k''}$. The TKE decrease ratios $1 - \bar{\rho}\widetilde{K}\big|_{\rm post} \Big/ \bar{\rho}\widetilde{K}\big|_{\rm pre}$ at $y^{+0} \approx 100$ for each flow condition are shown in Table 2. For all of the Reynolds numbers tested, the TKE decreases by a larger percentage for the low $\Delta p/\tau_{w0}$ (high Mach number) cases, where relaminarization is not expected according to the empirical condition by Narasimha & Viswanath (1975). The stronger relaminarization at the high Mach numbers indicate that relaminarization may be caused by the stronger expansion of the mean flow, not primarily by the favorable pressure gradient as Narasimha's parameter $\Delta p/\tau_{w0}$ suggests. In the following, we aim to model the TKE decrease through analyses of the TKE budget equation.

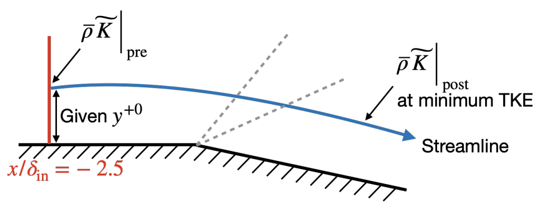

Figure 4. Schematic of the pre- and post-expansion locations along a given y^{+0}.

Table 2. TKE decrease ratio at $y^+ \approx 100$ for cases with $\alpha = 12°$.

Re_θ	$\frac{\Delta p}{\tau_{w0}} > 75$ (Low Mach)	$60 < \frac{\Delta p}{\tau_{w0}} < 75$ (Medium Mach)	$\frac{\Delta p}{\tau_{w0}} < 60$ (High Mach)
1000	0.783	0.814	0.838
3000	0.772	0.801	0.864
5000	0.775	0.830	0.852

Model for TKE decrease ratio

To elucidate how the rapid TKE decrease occurs, we show the production term of the TKE budget equation in Figure 5 (top), where we observe that the production term takes a negative value at the expansion corner. Although we do not show the other terms of the budget equation here, existing studies have shown that the change in the production term is the main driver of the reduction in TKE (Teramoto *et al.* (2017); Sun *et al.* (2017)). We also note that the near-wall positive production in the downstream region causes the rapid recovery of the near-wall TKE observed in Figures 2 and 3. In a similar fashion to Teramoto *et al.* (2017), we further decompose the production term into subterms as

$$-\bar{\rho}\widetilde{u_i''u_j''}\frac{\partial \tilde{u}_i}{\partial x_j} = \left(-\bar{\rho}\widetilde{u''u''}\frac{\partial \tilde{u}}{\partial x} - \bar{\rho}\widetilde{v''v''}\frac{\partial \tilde{v}}{\partial y}\right) + \left(-\bar{\rho}\widetilde{u''v''}\frac{\partial \tilde{u}}{\partial y} - \bar{\rho}\widetilde{u''v''}\frac{\partial \tilde{v}}{\partial x}\right), \qquad (1)$$

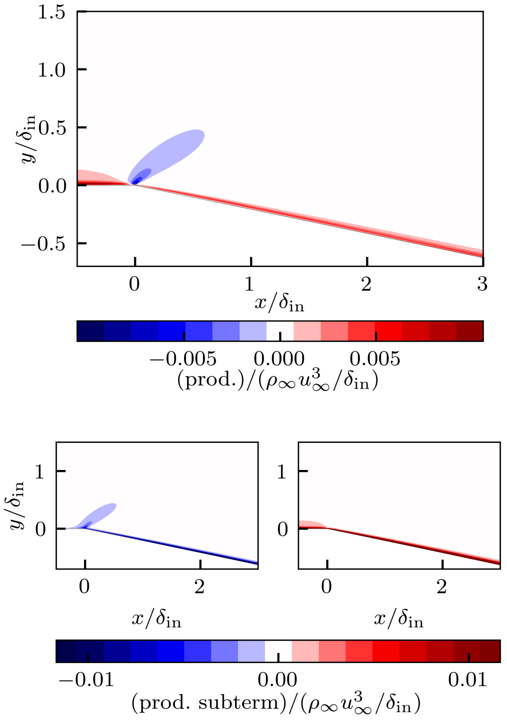

Figure 5. Distribution of production term of TKE budget (top) and its diagonal (bottom-left) and off-diagonal (bottom-right) components for $Re_\theta = 5000,\ M = 2,\ \alpha = 12^\circ$ case.

where the two terms in the right hand side are here named the diagonal and off-diagonal components, respectively. The diagonal and off-diagonal components of the production term are shown in Figure 5 (bottom). The negative production is mostly caused by the diagonal component. Considering the expression in Equation 1, the rise of the negative production is considered to be strongly correlated with both the components of the TKE $0.5\overline{\rho}\widetilde{u_k'' u_k''}$ and the mean flow divergence $\partial \widetilde{u}_k/\partial x_k$.

Based on the above observations, we formulate the model for the TKE decrease ratio. We base the modeling approach on the TKE budget equation which is expressed as

$$\frac{\partial \overline{\rho}\widetilde{K}}{\partial t} + \frac{\partial \overline{\rho}\widetilde{K}\widetilde{u}_k}{\partial x_k} = \sum_i (\mathrm{term}_i)\,, \tag{2}$$

where (term_i) represent the various terms in the budget equation such as production, dissipation, and diffusions. We rearrange the equation using the Lagrange derivative to obtain

$$\frac{D\overline{\rho}\widetilde{K}}{Dt} = -\overline{\rho}\widetilde{K}\frac{\partial \widetilde{u}_k}{\partial x_k} + \sum_i (\mathrm{term}_i)\,. \tag{3}$$

Here, we introduce a modeling assumption that each term can be written as

$$(\mathrm{term}_i) = C_i \overline{\rho}\widetilde{K}\frac{\partial \widetilde{u}_k}{\partial x_k} \tag{4}$$

with a constant C_i. This assumption is based on the above observation that the change in the TKE is predominantly caused by the negative production, which is largely correlated with the TKE and the mean flow expansion. The other terms are considered to be also strongly affected by the production term, and therefore the terms are modeled as a scalar multiple of the TKE and the mean velocity divergence. Under this assumption, by considering the time integral in a Lagrange sense from the pre-expansion state to the post-expansion state of Equation 3, we obtain

$$\int_{\mathrm{pre}}^{\mathrm{post}} \frac{D\overline{\rho}\widetilde{K}}{Dt} dt = \int_{\mathrm{pre}}^{\mathrm{post}} \left(\sum_i (C_i - 1)\overline{\rho}\widetilde{K}\frac{\partial \widetilde{u}_k}{\partial x_k} \right) dt, \tag{5}$$

$$\frac{\overline{\rho}\widetilde{K}\Big|_{\mathrm{pre}} - \overline{\rho}\widetilde{K}\Big|_{\mathrm{post}}}{\overline{\rho}\widetilde{K}\Big|_{\mathrm{pre}}} = 1 - \left(\frac{\overline{\rho}|_{\mathrm{post}}}{\overline{\rho}|_{\mathrm{pre}}} \right)^{-\sum_i C_i + 1}. \tag{6}$$

In this study, we model the constants C_i for each term by using the integral values as follows:

$$C_{i,\mathrm{model}} = \frac{\int_{\mathrm{pre}}^{\mathrm{post}} (\mathrm{term}_i) dt}{\int_{\mathrm{pre}}^{\mathrm{post}} \overline{\rho}\widetilde{K}\frac{\partial \widetilde{u}_k}{\partial x_k} dt}. \tag{7}$$

Figure 6 shows the modeled coefficients $C_{i,\mathrm{model}}$ for all computed cases in bar graphs. Much of the negative contributions come from the diagonal component of production and the dissipation. Remarkably, all cases take a similar value of $\sum_i C_{i,\mathrm{model}} \approx -2$. From Equation 6, we therefore use $\left(\overline{\rho}\widetilde{K}\Big|_{\mathrm{pre}} - \overline{\rho}\widetilde{K}\Big|_{\mathrm{post}} \right) \Big/ \overline{\rho}\widetilde{K}\Big|_{\mathrm{pre}} = 1 - \left(\overline{\rho}|_{\mathrm{post}}/\overline{\rho}|_{\mathrm{pre}}\right)^3$ as a potential model for the TKE decrease ratio. Here, $(\overline{\rho}|_{\mathrm{post}}/\overline{\rho}|_{\mathrm{pre}})$ can be estimated in an *a priori* manner from the flow parameters using the results of Prandtl–Meyer expansion theory.

In Figure 7, the proposed model equation is validated against the measured TKE decrease ratio at $y^{+0} \approx 100$. The markers representing each flow condition are placed near the diagonal line, showing good accuracy of the proposed model equation. The results suggest that $1 - \left(\overline{\rho}|_{\mathrm{post}}/\overline{\rho}|_{\mathrm{pre}}\right)^3$ is a dominant nondimensional parameter that characterizes the TKE decrease ratio, and can be used to estimate the extent of relaminarization quantitatively solely from the flow parameters.

CONCLUDING REMARKS

In this study, we have performed the direct numerical simulations of the relaminarizing turbulent boundary layers at supersonic expansion corners. The obtained skin friction coefficients and the distributions of the turbulent kinetic energy (TKE) suggest that relaminarization occurs for the present computed range of Reynolds and Mach numbers at the deflection angle of $\alpha = 12^\circ$, including the cases where relaminarization is not expected according to the existing Narasimha's parameter. Furthermore, a non-dimensional parameter for the TKE decrease ratio is derived through the analysis of the TKE budget equation. The proposed model parameter can be computed solely from the prescribed flow parameters, and is shown to agree well with the measured TKE decrease.

Acknowledgements

This work was supported in part by Japan Society for the Promotion of Science KAKENHI Grant Number 26H02169 and JST SPRING Grant Number JPMJSP2114. A part of the

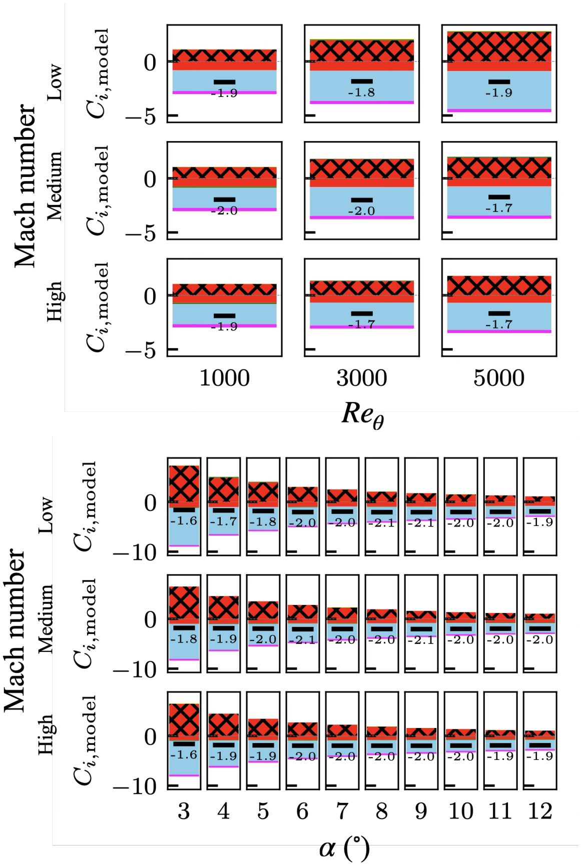

Figure 6. Model coefficients for varying Reynolds and Mach numbers for fixed $\alpha = 12°$ (top) and varying Mach number and deflection angles for fixed $Re_\theta = 1000$ (bottom). Red (hatched), production (diagonal component); red, production (off-diagonal component); blue, dissipation; green, diffusion; yellow, pressure-dilation; magenta, mass flux contributions. Black horizontal marks and the numerical values within each graph denote the sum of all terms.

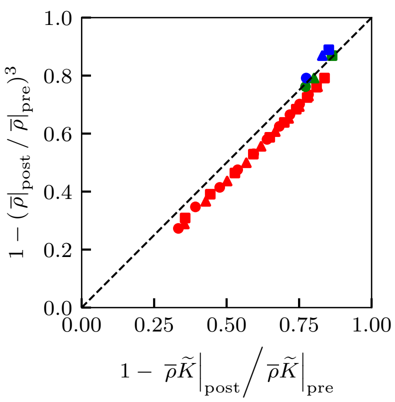

Figure 7. Measured TKE decrease ratio versus proposed model. Red, $Re_\theta = 1000$; green, $Re_\theta = 3000$; blue, $Re_\theta = 5000$. Circles, low Mach; triangles, medium Mach; squares, high Mach.

computations in this study was conducted by using the computational resources of a supercomputer Fugaku provided by the RIKEN Center for Computational Science through the HPCI System Research Project (project ID: hp240083, hp250090, hp260108).

REFERENCES

Gaitonde, Datta V & Visbal, Miguel R 2000 Padé-type higher-order boundary filters for the Navier–Stokes equations. *AIAA journal* **38** (11), 2103–2112.

Goldfeld, Marat Abramovich, Nestoulia, Roman Vladimirovich & Shiplyuk, Aleksandr Nikolaevich 2002 Relaminarization of a turbulent boundary layer with a mach number m ∞ = 4. *Journal of applied mechanics and technical physics* **43** (1), 76–82.

Gottlieb, S. & Shu, C. W. 1998 Totalvariation diminishing runge-kutta schemes. *Mathmatics of computation of the American Mathematical Society* pp. 73–85.

Lele, Sanjiva K 1992 Compact finite difference schemes with spectral-like resolution. *Journal of computational physics* **103** (1), 16–42.

Narasimha, R & Viswanath, PR 1975 Reverse transition at an expansion corner in supersonic flow. *AIAA Journal* **13** (5), 693–695.

Nguyen, Tue, Behr, Marek, Reinartz, Birgit, Hohn, Oliver & Gülhan, Ali 2013 Effects of sidewall compression and relaminarization in a scramjet inlet. *Journal of Propulsion and Power* **29** (3), 628–638.

Pandey, Anshuman, Casper, Katya M & Beresh, Steven J 2024 Relaminarization effects in hypersonic flow on a three-dimensional expansion–compression geometry. *Journal of Fluid Mechanics* **985**, A25.

Sun, Ming-bo, Hu, Zhiwei & Sandham, Neil D 2017 Recovery of a supersonic turbulent boundary layer after an expansion corner. *Physics of Fluids* **29** (7).

Teramoto, Susumu, Sanada, Hiroki & Okamoto, Koji 2017 Dilatation effect in relaminarization of an accelerating supersonic turbulent boundary layer. *AIAA Journal* **55** (4), 1469–1474.

Urbin, Gerald & Knight, Doyle 2001 Large-eddy simulation of a supersonic boundary layer using an unstructured grid. *AIAA Journal* **39** (7), 1288–1295.

Volino, Ralph J 2020 Non-equilibrium development in turbulent boundary layers with changing pressure gradients. *Journal of Fluid Mechanics* **897**, A2.